Design of Mid-IR Er^{3+}-Doped Microsphere Laser

L. Mescia
P. Bia
O. Losito
F. Prudenzano
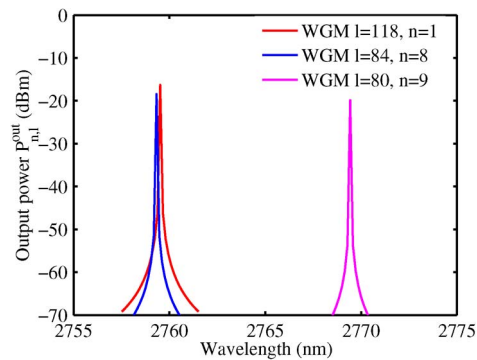
Design of Mid-IR Er³⁺-Doped Microsphere Laser

L. Mescia, P. Bia, O. Losito, and F. Prudenzano

Dipartimento di Ingegneria Elettrica e dell'Informazione (DEI), Politecnico di Bari, 70125 Bari, Italy

Abstract: A mid-IR lasing system based on a tapered fiber coupled to an Er³⁺-doped microsphere has been modeled and numerically investigated. In order to design and optimize the device performance, a dedicated 3-D numerical code exploiting the coupled mode theory and the rate equations model has been developed. The main energy level transitions among the Er³⁺ ions, the most relevant secondary ion–ion interactions, the amplified spontaneous emission, and the fiber-microsphere coupling phenomena have been taken into account. In order to optimize the lasing performance, several parametric simulations have been carried out. The obtained numerical results show that a laser threshold of about 55 mW and an output power of about −17.8 dBm can be obtained by using small microspheres.

Index Terms: Whispery gallery mode, resonator, coupled mode theory, optical device, erbium.

1. Introduction

During the last years, optical micro- and nanospheres have attracted more attention because their striking properties such as high Q-quality factor (higher than 10^9) and flexible choice of resonator material. These properties make dielectric microspheres interesting for numerous high-performance photonic devices, including advanced active devices [1]–[3], quantum information processing [1], nonlinear optics, cavity quantum electrodynamics (QED), and ultrasensitive molecular sensors [4], [5]. Moreover, dielectric microspheres are under consideration to be used as elements in integrated devices.

A significant success has been achieved in the fabrication of glass-based spherical micro-resonators because of i) the relative easiness of fabricating high-purity glasses with ultralow absorption losses [6], ii) the microresonator feasibility by relatively simple and low cost fabrication processes [6].

The electromagnetic field sustained by a dielectric microsphere, called whispering gallery mode (WGM), exhibits a high quality factor and small modal volume. As a consequence, it makes possible a good optical energy storage and an enhancement of the light-matter interaction allowing the lasing action when the microsphere is doped with rare earth ions. In particular, many research efforts in rare earth doped microspheres have opened novel opportunities for enhancing the amplifier and laser performance, especially in the mid-IR wavelength range [1], [2], and [6]–[8].

Laser oscillation has been observed in near-IR wavelengths by using microspheres based on silica glass host materials [9]–[11]. However, because of the strong increasing of the multiphonon absorption for wavelength higher than 2 μm, silica microspheres cannot be used for mid-IR

applications. Among the low-phonon energy glasses, chalcogenide ones are promising candidates to overcome this drawback [6], [8], [12]. In fact, they are suitable lasing and amplifying materials because of their high refractive index, higher capability to host rare-earth ions like erbium, low phonon energy and infrared transparency. These properties could allow the development of a new generation of coherent sources in mid-IR wavelength range. Even if many mathematical models of both passive [13], [14] and active microsphere have been developed [1], [2] [15]–[17], more accurate models are essential for design and analysis purposes. In fact, experimental research requires good numerical tools to study the light-matter interaction inside the microsphere and to design optimized amplifying and lasing systems. To this aim, for the first time to the best of our knowledge, in this paper we propose a detailed 3D mathematical model allowing the performance evaluation of the laser constituted by a tapered fiber coupled to the Er^{3+}-doped chalcogenide $(Ga_5Ge_{20}Sb_{10}S_{65})$ glass microsphere. The model takes into account i) the stimulated emission at the signal wavelength; ii) the radiative and nonradiative rates among the Er^{3+}-energy levels, at both the pump and the signal wavelengths; iii) the Er^{3+}-energy level lifetimes; iv) the amplified spontaneous emission (ASE) noise around the signal wavelength; v) the ion-ion energy transfers; vi) the modal electromagnetic field propagation of several WGMs; and vii) the evanescent field interaction between optical fiber and microsphere. The obtained results show that, by using a pump signal at the wavelength $\lambda_p = 980$ nm, a lasing action in the wavelength range from 2740 nm to 2820 nm can be achieved.

2. Theoretical Analysis

An accurate electromagnetic analysis has been performed. In particular, the modal electromagnetic field distribution and the z-depending propagation constant of the guided modes of the tapered optical fiber have been calculated by using the local modal theory [18], while the spatial electromagnetic field profiles and propagation constants of WGMs have been evaluated by solving the scalar Helmholtz equation in spherical coordinates [19]:

$$\frac{1}{r^2}\frac{\partial}{\partial r}\left(r^2\frac{\partial\psi}{\partial r}\right) + \frac{1}{r^2\sin\theta}\frac{\partial}{\partial\theta}\left(\sin\theta\frac{\partial\psi}{\partial\theta}\right) + \frac{1}{r^2\sin^2\theta}\frac{\partial^2\psi}{\partial\varphi^2} + k^2 n_s^2\psi = 0 \tag{1}$$

where $k = 2\pi/\lambda$ is the wavenumber, n is the refractive index of the microsphere, and ψ is the electric or magnetic field.

In particular, the azimuthal, polar and radial electromagnetic field distributions of WGMs are given by the complex exponential functions, Hermite polynomials and spherical Bessel functions, respectively. Thus each WGM can be identified by three integers l, m, n. In the developed numerical code, several WGMs, in the signal wavelength range from 2740 nm to 2820 nm, and the fundamental WGM ($l = 352$, $m = 352$, $n = 1$), at the pump wavelength $\lambda_p = 980$ nm, have been taken into account.

Many parametric simulations have been performed to find the optimal geometrical parameters of both the microsphere and the tapered fiber, maximizing a) the pump power circulating in the microsphere and b) the laser signal power transmitted through the coupled tapered fiber. In particular, the considered parameters are the fiber-microsphere gap g, the microsphere radius R_0, the fiber waist radius a, the taper angle δ, the erbium concentration N_{Er} and the thickness of the doped region S. In order to obtain reliable numerical results, the doped region has been discretized in α sector, having radial amplitude Δr and polar amplitude $\Delta\theta$, on the $\hat{\mathbf{r}} \cdot \hat{\theta}$ plane.

Fig. 1 shows the Er^{3+}-energy level transitions considered in the developed numerical code. In particular, by using a pump signal at the wavelength $\lambda_p = 980$ nm, it is possible to generate a population inversion between the Er^{3+}-energy levels $^4I_{11/2}$ and $^4I_{13/2}$. In fact, because of the quite high dopant concentration and the comparable lifetime of the $^4I_{13/2}$, $^4I_{11/2}$, $^4I_{9/2}$ energy levels, a stimulated emission can occur in the wavelength range from 2740 nm to 2820 nm, i.e., where the erbium emission cross section exhibits a peak. Moreover, nonlinear processes due to the ion-ion interaction such as uniform cooperative up-conversion $(^4I_{13/2}, {}^4I_{13/2} \rightarrow^4 I_{15/2}, {}^4I_{9/2})$, $(^4I_{11/2}, {}^4I_{11/2} \rightarrow^4 I_{15/2}, {}^4S_{3/2})$, $(^4I_{9/2}, {}^4I_{9/2} \rightarrow^4 S_{3/2}, {}^4I_{13/2})$ and cross-relaxation $(^4I_{15/2}, {}^4I_{9/2} \rightarrow^4 I_{13/2})$, $(^4I_{15/2}, {}^4S_{3/2} \rightarrow^4 I_{9/2}, {}^4I_{13/2})$, $(^4I_{15/2}, {}^4S_{3/2} \rightarrow^4 I_{13/2}, {}^4I_{9/2})$, $(^4I_{13/2}, {}^4I_{9/2} \rightarrow^4 I_{15/2}, {}^4S_{3/2})$ have been

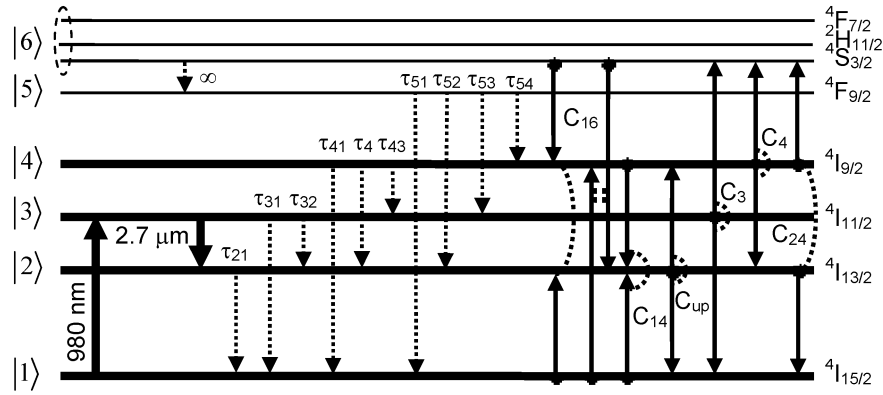Fig. 1. Er^{3+}-energy level transitions taken into account in the numerical model.

considered, too. The transition labeled with the symbol ∞ is assumed to be instantaneous decays yielding a complete depopulation of the energy levels $^4F_{7/2}$, $^1H_{11/2}$ and $^4S_{3/2}$.

The modeling of the microsphere laser requires the calculation of the coupling coefficients, describing the electromagnetic interaction between the fiber and the microsphere; the quality factor, depending on the microsphere losses; the overlap factor, describing the overlap between the modal field of the WGMs and the microsphere doped region; the transmission coefficient of the coupled waveguide system and circulating power in the microsphere; the transition rates among the Er^{3+}-energy levels. To evaluate the device performance, the lasing output power has been calculated as a sum of the amplitude of each degenerate mode by using the equation:

$$P_{l,n}^{out}(t) = \frac{1}{2Z_0}\left| \sum_{m=l-1}^{l} n_{l,m,n}^{eff}\sqrt{\frac{T_{l,m,n}^c}{\tau_{l,m,n}^{ext}}}A_{l,m,n}^s(t) \right|^2 \tag{2}$$

where $T_{l,m,n}^c = 2\pi R_0 n_{l,m,n}^{eff}/c$ is the circulating time inside the microsphere (round trip time), $\tau_{l,m,n}^{ext} = 1/(\kappa_{l,m,n}^{ext})^2 = m\pi(\omega K)^2$ is the coupling lifetime, $A_{l,m,n}^s(t)$ is the time-depending field amplitude inside the microsphere, $n_{l,m,n}^{eff}$ is the WGM effective refractive index. In particular, $n_{l,m,n}^{eff}$ has been calculated by solving the characteristic equation obtained by matching the tangential components of electric and magnetic fields at the sphere boundary [1], [19]. Moreover, $Z_0 = 377\ \Omega$ is the vacuum characteristic impedance, K is the overlap factor between the WGM and the fundamental mode of the fiber, given by:

$$K = \frac{k^2(n_s^2 - n_0^2)}{2}\int_V \frac{\mathbf{E}_f \cdot \mathbf{E}_s^*}{\beta_f}dV \tag{3}$$

where β_f is the z-depending phase constant of the optical fiber mode, n_0 is the background refractive index, $\mathbf{E}_f$ and $\mathbf{E}_s$ are the electric field of the fiber fundamental mode and the WGM, respectively, both normalized on the $\hat{\mathbf{r}} \cdot \hat{\theta}$ plane [1], [19]. Finally, in eq. (2), the lasing output power is obtained by considering the power of all degenerate lasing modes, such that $l - 1 \le m \le l$. By dividing the doped area on the $\hat{\mathbf{r}} \cdot \hat{\theta}$ plane in α sectors, the overlap factor of each WGM with the rare-earth profile corresponding to the α-th sector is:

$$\Gamma_{l,m,n}^{\alpha} = \int\int_{S_\alpha} \left| E_{l,n}(r,\theta)e^{-jm\varphi} \right|^2 rdrd\theta \tag{4}$$

where S_α is the area of the α-th sector.

The field amplitude evolution of both pump $(A^p_{l,m,n})$ and lasing $(A^s_{l,m,n})$ signals are obtained by solving the following coupled differential equation [1]:

$$\frac{dA^p_{l,m,n}}{dt} = -\frac{1}{2}\left(\frac{1}{\tau^{ext,p}_{l,m,n}} + \frac{1}{\tau^{0,p}_{l,m,n}} - g^p_{l,m,n} - 2i\Delta\omega^p\right) \times A^p_{l,m,n} + i\sqrt{\frac{1}{\tau^{ext,p}_{l,m,n}T^c_{l,m,n}}}A^p_{in,l,m,n}$$

$$\frac{dA^s_{l,m,n}}{dt} = -\frac{1}{2}\left(\frac{1}{\tau^{ext,s}_{l,m,n}} + \frac{1}{\tau^{0,s}_{l,m,n}} - g^s_{l,m,n}\right) \times A^s_{l,m,n} + \frac{c}{2n^{eff}_s}A^0_{l,m,n}\sigma_{32}(\nu_{l,m,n})\sum_\alpha N^\alpha_3 \Gamma^{\alpha,s}_{l,m,n} \qquad (5)$$

where $\Delta\omega^p = \omega^p_{WGM} - \omega^p_{in}$ is the frequency detuning between the excitation frequency ω^p_{in} of the pump signal and the corresponding resonance frequency ω^p_{WGM} of the WGM; $\tau^{0,p}_{l,m,n}$ and $\tau^{0,s}_{l,m,n}$ are the intrinsic lifetime at the pump and signal wavelengths, respectively; N^α_3 is the ion population of the $^4I_{11/2}$ energy-level in the α-th sector; $g^a_{l,m,n}$ $(a = s, p)$ is the gain amplification calculated by using the following equation [1]:

$$g^s_{l,m,n} = \frac{c}{n^{eff}_{l,m,n}}\sum_\alpha\left\{\Gamma^{\alpha,s}_{l,m,n}\left[N^\alpha_3\sigma_{32}(\nu_{l,m,n}) - N^\alpha_2\sigma_{23}(\nu_{l,m,n})\right]\right\} \qquad (6)$$

$$g^p_{l,m,n} = \frac{c}{n^{eff}_{l,m,n}}\sum_\alpha\left\{\Gamma^{\alpha,p}_{l,m,n}\left[N^\alpha_3\sigma_{31}(\nu_{l,m,n}) - N^\alpha_1\sigma_{13}(\nu_{l,m,n})\right]\right\} \qquad (7)$$

where $\sigma_{13}(\nu_{l,m,n})$ and $\sigma_{31}(\nu_{l,m,n})$ are the absorption and emission cross sections between levels 1 and 3 at the pump wavelength, respectively; $\sigma_{23}(\nu_{l,m,n})$ and $\sigma_{32}(\nu_{l,m,n})$ are the absorption and emission cross sections between levels 2 and 3 at the signal wavelength, respectively; $\Gamma^{\alpha,s}_{l,m,n}$ and $\Gamma^{\alpha,p}_{l,m,n}$ are the overlap factors of each WGM in the α-th sector at the pump and the signal wavelength, respectively. $A^0_{l,m,n}$ represent the ASE contributions due to a single photon in the bandwidth $\Delta\nu_{l,m,n}$, given by:

$$A^0_{l,m,n} = (2h\nu_{l,m,n}\Delta\nu_{l,m,n})/\left(A^s_{l,m,n}cn^{eff}_{l,m,n}\varepsilon_0\right) \qquad (8)$$

$\Delta\nu_{l,m,n}$ is the FWHM (full width at half maximum) resonance bandwidth defined as [14]:

$$\Delta\nu_{l,m,n} = FWHM = \frac{1}{2\pi\tau^{ext,s}_{l,m,n}} + \frac{1}{2\pi\tau^{0,s}_{l,m,n}} . \qquad (9)$$

In order to take into account the lasing phenomenon, eq. (5)–(8) have been achieved by means of a suitable extension of the theoretical model regarding the amplification system illustrated in [1]. To this aim, the initial condition related to the presence of the input wave to amplify has been removed, and only the ASE contribution is considered. Moreover, to identify the actual spectrum of the emitted light 100 WGMs $(n = 1, 2, \ldots, 16; m = l, l - 1)$ have been simultaneously considered in eq. (5)–(8). In this way, it is possible to simulate the intermode coupling and calculate the actual WGMs involved in the lasing.

3. Numerical Results

The implemented 3D numerical code requires less computational resources compared with the other algorithms based on FDTD (Finite Difference Time Domain), FEM (Finite Element Method) and BPM (Beam Propagation Method). The developed numerical code is very flexible and provides reliable results. Moreover, it allows the calculation of the temporal evolution of the optical signals inside the microsphere and at the output of the fiber taper as well as the investigation of several device configurations. In order to design a device having high performance in terms of lasing power and laser threshold, many simulations have been carried out. In the calculation, about 100 different WGMs, spanning the signal band from 2740 nm to 2820 nm, have been taken into account. The considered refractive index of the microsphere at both pump and signal wavelengths are $n_s(\lambda_p) = 2.275$ and $n_s(\lambda_s) = 2.225$, respectively. However, by taking into account microsphere radius $R_0 = 25\ \mu m$, fiber radius $a = 700$ nm, taper angle $\delta = 0.03$ rad, fiber-microsphere gap
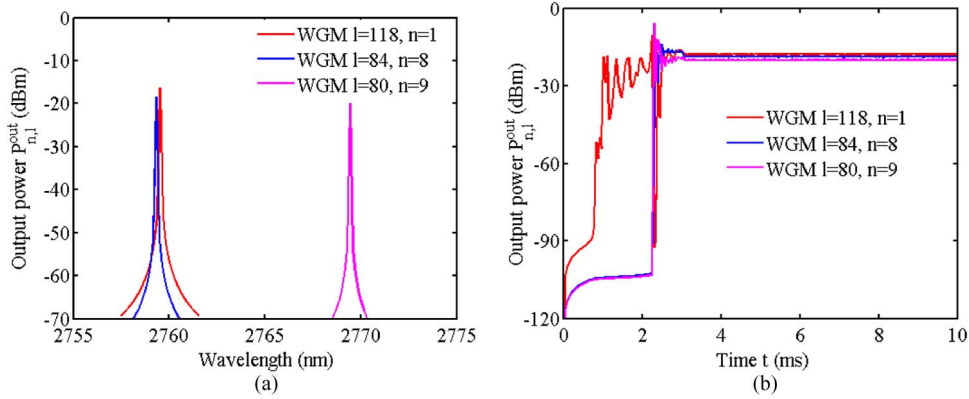
Fig. 2. (a) Laser spectrum at the fiber taper output and (b) temporal evolution of the output laser power for the three lasing WGMs for an input pump power of 100 mW, microsphere radius $R_0 = 25$ μm, fiber-microsphere gap $d = 560$ nm, erbium concentration $N_{Er} = 0.5$ w%, taper angle $\delta = 0.03$ rad, thickness of the doped region $S = 3$ μm.

$d = 560$ nm, erbium ions concentration $N_{Er} = 0.5$ w%, we verified that only three WGMs result in microsphere lasing: WGM ($l = 118$, $n = 1$) at $\lambda_{118,1} = 2759.5$ nm, WGM ($l = 84$, $n = 8$) at $\lambda_{84,8} = 2759.3$ nm and WGM ($l = 80$, $n = 9$) at $\lambda_{80,9} = 2769.4$ nm. Fig. 2(a) shows the spectrum of the laser emission appearing at output of the fiber taper for an input pump power $P_{in} = 100$ mW and thickness of doped region $S = 3$ μm. It is worthwhile to note that for all the WGMs, a microsphere laser output of about -20 dBm is calculated. Moreover, for each peak, a low FWHM has been calculated: 163.4 MHz for WGM ($l = 118$, $n = 1$), 34.2 MHz for WGM ($l = 84$, $n = 8$) and 32.3 MHz for WGM ($l = 80$, $n = 9$). Fig. 2(b) depicts the time domain evolution of the output lasing power. It can be observed that all the three WGMs exhibit a lasing operation after a time delay of about 4 ms. The time required to build up the laser signal depends on the order of the WGM and on input pump power. In particular, the regime condition is reached after about 4 ms, and the corresponding lasing power are: $P_{out}^{118,1} = -17.8$ dBm for WGM ($l = 118$, $n = 1$), $P_{out}^{84,8} = -18.7$ dBm for WGM ($l = 84$, $n = 8$) and $P_{out}^{80,9} = -20$ dBm for WGM ($l = 80$, $n = 9$). Moreover, the time required to build up the laser signal decreases by increasing the pump power.

The variation of the lasing performance due to the changes of the taper angle and fiber radius has been investigated, too. In fact, a proper design of these parameters ensures the fundamental mode propagation along the waveguide formed by the fiber waist surrounded by air, allowing a significant evanescent field into the space surrounding the taper. Moreover, the fiber radius should be tailored in order to efficiently couple the pump beam into the rare earth-doped microsphere and to enhance the extraction of the lasing signal from the microsphere. Fig. 3(a) shows the dependence of the output power as a function of the taper angle. For taper angle lower than 0.012 rad, the pump signal cannot generate the population inversion since it is poorly coupled with the microsphere. For taper angle in the range $0.01 \div 0.022$ rad, only the lasing of the fundamental WGM ($l = 118$, $n = 1$) takes place, and the output power associated to this resonance increases by increasing the taper angle. In this case, the normalized coupling coefficient $K = \tau_{l,m,m}^{0,s} / \tau_{l,m,m}^{ext,s}$ varies from about 370 to about 380 for WGM ($l = 118$, $n = 1$) and takes a quite constant value of about 60 for WGM ($l = 84$, $n = 8$) and WGM ($l = 80$, $n = 9$). However, even if WGM ($l = 118$, $n = 1$) works in a stronger overcoupling regime with respect to the other two WGMs, it is the only one exhibiting lasing since its fully overlapping with the doped region. For taper angle higher than 0.022 rad, a simultaneous lasing action arises for three different WGMs. In this operation regime, the normalized coupling coefficient of the WGM ($l = 118$, $n = 1$) is much too high, and as a consequence, the other two WGMs, even if poorly overlapped with the doped region, can compete with the fundamental one. Moreover, due to the strong modal competition, for taper angle higher than 0.035 rad, the WGM ($l = 118$, $n = 1$) transfers part of its power to WGM ($l = 84$, $n = 8$) and WGM ($l = 80$, $n = 9$). However, taking into account the fiber waist radius used in the simulations, taper angles in the range $0.01 \div 0.022$ allow
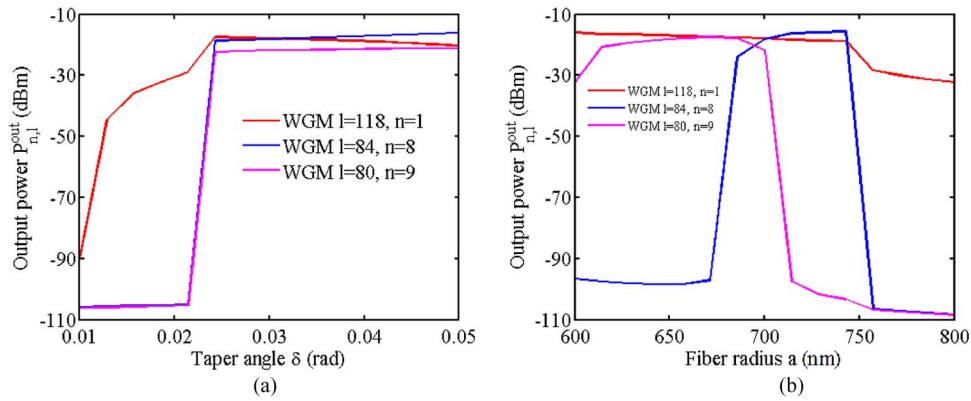
Fig. 3. (a) Output laser power versus the taper angle and (b) versus the fiber radius for an input pump power of 100 mW, microsphere radius $R_0 = 25$ μm, fiber-microsphere gap $d = 560$ nm, erbium concentration $N_{Er} = 0.5$ w%, thickness of the doped region $S = 3$ μm.
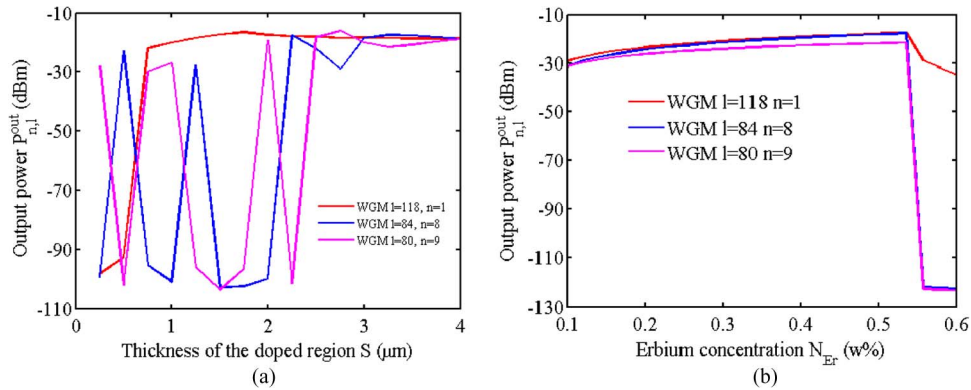

Fig. 4. (a) Output laser power versus the thickness of the doped region and (b) versus the erbium concentration for an input pump power of 100 mW, microsphere radius $R_0 = 25$ μm, fiber-microsphere gap $d = 560$ nm, taper angle $\delta = 0.03$ rad, fiber radius $a = 700$ nm.

a good fiber-microsphere coupling and an easily taper manufacturing by using conventional methods for tapering optical fibers.

Fig 3(b) illustrates the dependence of the output power as a function of the fiber radius. It is worthwhile to note that for fiber radius higher than 750 nm, a lasing action occurs only for WGM ($l = 118$, $n = 1$). All the WGMs work in overcoupling regime. However, even if WGM ($l = 118$, $n = 1$) is stronger overcoupled it dominates on the other ones because of its higher overlapping with the doped region. As result, for fiber radius in the range $740 \div 800$ nm, it exhibits an output power varying from -19 dBm to -32 dBm. For the fiber radius in the range 650 nm $\div$ 750 nm, only WGM ($l = 118$, $n = 1$) exhibits a stable lasing action, while the oscillating behavior of the other two WGMs indicates a modal competition between them.

Fig. 4(a) illustrates the output power associated with three WGM as a function of the thickness of the doped region S and for input pump power $P_{in} = 100$ mW and erbium concentration $N_{Er} = 0.5$ w%. It can be observed that for thickness of the doped region higher than 3 μm, a lasing action occurs for all the three WGMs. In this case, by considering that $\Gamma_{118,1} = 0.99$, the WGM ($l = 118$, $n = 1$) is fully overlapped with the doped region and, because $K_{118,1} = 454$, it works in a strong overcoupling regime. At the same time, even if less overlapped with the doped region ($\Gamma_{84,8} = 0.2$, $\Gamma_{80,9} = 0.18$) the WGM ($l = 84$, $n = 8$) and WGM ($l = 80$, $n = 9$) exhibit a comparable output power because their lower values of the normalized coupling coefficient ($K_{84,8} = 67$, $K_{80,9} = 60$). For the thickness S in the
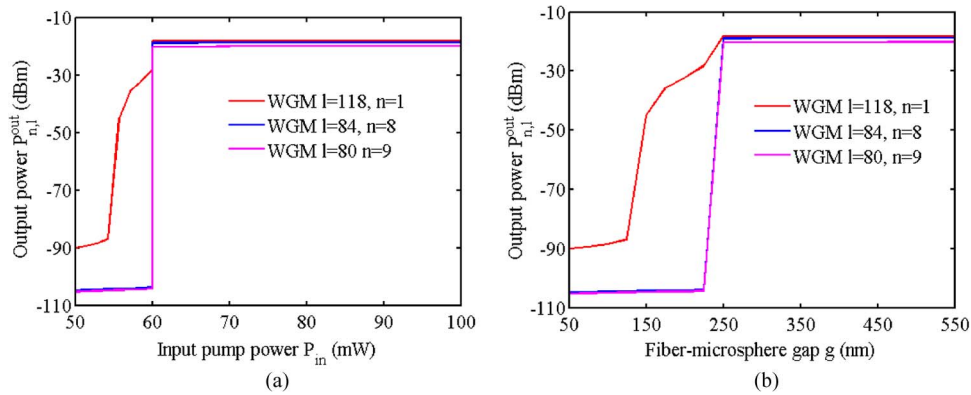
Fig. 5. (a) Output laser power versus the input one and (b) versus the fiber-microsphere gap for microsphere radius $R_0 = 25\ \mu$m, erbium concentration $N_{Er} = 0.5$ w%, taper angle $\delta = 0.03$ rad, fiber radius $a = 700$ nm, thickness of the doped region $S = 3\ \mu$m.

range $0.8\ \mu$m $\div$ $3\ \mu$m, only WGM ($l = 118$, $n = 1$) exhibits a stable lasing action, while it is apparent the modal competition between the other two WGMs. Fig. 4(b) illustrates the output power as a function of the erbium concentration for $S = 3\ \mu$m. For all the three lasing WGMs, the output power increases by increasing the erbium concentration showing a peak for $N_{Er} \approx 0.53$ w%. In this condition, the pump signal circulating in the microsphere is high enough to ensure a strong population inversion whose value mainly depends on erbium concentration. For $N_{Er} > 0.53$ w%, the nonlinear effects due to the upconversion phenomena became more efficient, and higher pump power is required to fully invert the active medium. As result, the threshold pump power required to activate the laser action increases by increasing the erbium concentration becoming higher than 100 mW.

Fig. 5(a) shows the lasing power as function of input pump power using a fiber-microsphere gap $d = 560$ nm. For pump powers lower than 55 mW, no lasing occurs because the pump power is not high enough to generate the ion population inversion. In fact, in this operation regime, the absorption rate due to the internal cavity field at the pump wavelength induces a weak population improvement of the $^4I_{11/2}$ energy level. As a consequence, only ASE spectrum can be collected at the fiber output end. For pump power in the range 55 mW $\div$ 60 mW, only the lasing of the fundamental WGM ($l = 118$, $n = 1$) takes place, and the output power associated to this resonance increases with pump power. For pump power higher than 60 mW, a simultaneous lasing action arises for three different WGMs: WGM ($l = 118$, $n = 1$) with output power $P_{out}^{118,1} = -17.8$ dBm, WGM ($l = 84$, $n = 8$) with output power $P_{out}^{84,8} = -18.7$ dBm and WGM ($l = 80$, $n = 9$) with output power $P_{out}^{80,9} = -20$ dBm. All the other WGMs are not shown because their lasing power is lower than -90 dBm. The different values of the threshold pump power can be explained by taking into account the overlap and coupling factors. In fact, for the high order WGMs, the reduced overlap factor does not have enough ion population of the $^4I_{13/2}$ allowing the laser emission. On the other hand, for input pump powers higher than the threshold one, a strong ion population of the $^4I_{11/2}$ occurs. Moreover, for input pump power higher than 60 mW, the output power is quite constant because the active medium is fully inverted. However, the threshold pump power mainly depends on erbium concentration, thickness of the doped region, and fiber-microsphere gap. In fact, variations in these parameters change the overlap factor of each WGM with the rare-earth profile, the overlap factor between the WGM and the fundamental mode of the fiber, and the population inversion between the Er^{3+}-energy levels $^4I_{11/2}$ and $^4I_{13/2}$.

Fig. 5(b) illustrates the output laser power versus the fiber-microsphere gap. For gaps lower than 150 nm, the energy circulating in the microsphere poorly interacts with the active ions because both the pump and lasing signals work in a regime where the coupling is stronger than the loss. As result, a large portion of circulating power is coupled out to the fiber. By increasing the gap, a strong pump absorption rate occurs since most part of the pump signal is coupled into the microsphere. In this

way, a strong population inversion takes place, and a lasing signal can be collected at the fiber output end.

4. Conclusion

For the first time, to the best of our knowledge, a mid-infrared lasing system based on a tapered fiber coupled to an Er^{3+}-doped chalcogenide microsphere has been modeled and numerically investigated. In order to design and optimize the device performance, a dedicated 3D numerical code exploiting the coupled mode theory and rate equations has been developed. The obtained results highlight that the developed 3D numerical code is a useful tool to evaluate the lasing performance and to calculate the temporal evolution of the optical signals inside the microsphere by considering several device configurations. Numerous parametric simulations have been carried out to optimize the lasing performance. The obtained numerical results show that a laser threshold of about 55 mW can be obtained with lasing power of -17.8 dBm.

References

[1] L. Mescia, P. Bia, M. De Sario, A. Di Tommaso, and F. Prudenzano, "Design of mid-infrared amplifiers based on fiber taper coupling to erbium-doped microspherical resonator," *Opt. Exp.*, vol. 20, no. 7, pp. 7616–7629, Mar. 2012.
[2] P. Bia, A. Di Tommaso, and M. De Sario, "Modeling of mid-IR amplifier based on a erbium-doped chalcogenide microsphere," *Int. J. Opt.*, vol. 2012, pp. 1–5, 2012.
[3] L. Yang and J. Vahala, "Gain functionalization of silica microresonators," *Opt. Lett.*, vol. 28, no. 8, pp. 592–594, Apr. 2003.
[4] R. Hai-Cang, F. Vollmer, S. Arnold, and A. Libchaber, "High-Q microsphere biosensor—Analysis for adsorption of rodlike bacteria," *Opt. Exp.*, vol. 15, no. 25, pp. 17 410–17 423, Dec. 2007.
[5] F. Vollmer and A. Stephen, "Whispering-gallery-mode biosensing: Label-free detection down to single molecules," *Nat. Methods*, vol. 5, no. 7, pp. 591–596, Jul. 2008.
[6] B. Way, R. K. Jain, and M. Hossein-Zadeh, "High-Q microresonators for mid-IR light sources and molecular sensors," *Opt. Lett.*, vol. 37, no. 21, pp. 4389–4391, Nov. 2012.
[7] L. Xiao, S. Trebaol, Y. Dumeige, Z. Cai, M. Mortier, and P. Féron, "Miniaturized optical microwave source using a dual-wavelength whispering gallery mode laser," *IEEE Photon. Technol. Lett.*, vol. 22, no. 8, pp. 559–561, Apr. 2010.
[8] G. R. Elliott, G. S. Murugan, J. S. Wilkinson, M. N. Zervas, and D. W. Hewak, "Chalcogenide glass microsphere laser," *Opt. Exp.*, vol. 18, no. 25, pp. 26 720–26 727, Dec. 2010.
[9] G. S. Murugan, M. N. Zervas, Y. Panitchob, and J. S. Wilkinson, "Integrated Nd-doped borosilicate glass microsphere laser," *Opt. Lett.*, vol. 36, no. 1, pp. 73–75, Jan. 2011.
[10] M. Cai, O. Painter, K. J. Vahala, and P. C. Sercel, "Fiber-coupled microsphere laser," *Opt. Lett.*, vol. 25, no. 19, pp. 1430–1432, Oct. 2000.
[11] C. H. Dong, Y. Yang, Y. L. Shen, C. L. Zou, F. W. Sun, H. Ming, G. C. Guo, and Z. F. Han, "Observation of microlaser with Er-doped phosphate glass coated microsphere pumped by 780 nm," *Opt. Commun.*, vol. 282, no. 24, pp. 5117–5120, Dec. 2010.
[12] G. R. Elliot, D. W. Hewak, G. Senthil Murugan, and J. S. Wilkinson, "Chalcogenide glass microspheres; their production, characterization and potential," *Opt. Exp.*, vol. 15, no. 26, pp. 17 542–17 553, Dec. 2007.
[13] M. L. Gorodetsky and V. S. Ilchenko, "Optical microsphere resonators: Optimal coupling to high-Q whispering-gallery modes," *J. Opt. Soc. Amer. B, Opt. Phys.*, vol. 16, no. 1, pp. 147–154, Jan. 1999.
[14] C.-L. Zou, Y. Yang, C.-H. Dong, Y.-F. Xiao, X.-W. Wu, Z. F. Han, and G.-C. Guo, "Taper-microsphere coupling with numerical calculation of coupled-mode theory," *J. Opt. Soc. Amer. B, Opt. Phys.*, vol. 25, no. 11, pp. 1895–1898, Nov. 2008.
[15] L. Mescia, F. Prudenzano, M. De Sario, T. Palmisano, M. Ferrari, and G. C. Righini, "Design of rare-earth-doped microspheres," *IEEE Photon. Technol. Lett.*, vol. 22, no. 6, pp. 422–424, Mar. 2010.
[16] T. Kouki and T. Makoto, "Optical microsphere amplification system," *Opt. Lett.*, vol. 32, no. 21, pp. 3197–3199, Nov. 2007.
[17] Y. G. Boucher and P. Féron, "Generalizad transfer function: A simple model applied to active single-mode microring resonators," *Opt. Commun.*, vol. 282, no. 19, pp. 3940–3947, Oct. 2009.
[18] A. W. Snyder and J. D. Love, *Optical Waveguide Theory*. London, U.K.: Chapman & Hall, 1988.
[19] B. E. Little, J. P. Laine, and H. A. Haus, "Analytic theory of coupling from tapered fibers and half-blocks into microsphere resonators," *J. Lightwave Technol.*, vol. 17, no. 4, pp. 704–715, Apr. 1999.
[20] K. Vahala, *Optical Microcavities*. Singapore: World Scientific, 2004.